



Electrical and magnetic properties of chitosan-magnetite nanocomposites

Aarti S. Bhatt, D. Krishna Bhat*, M.S. Santosh

Department of Chemistry, National Institute of Technology Karnataka, Surathkal, Mangalore-575025, India

ARTICLE INFO

Article history:

Received 21 November 2009

Received in revised form

16 January 2010

Accepted 19 January 2010

Keywords:

Magnetic composites

Chitosan

Magnetite

Saturation magnetization

Dielectric properties

ABSTRACT

Magnetite powders in nanometer size have been synthesized by the hydrothermal process. Various magnetic films of chitosan and the synthesized magnetite nanopowders containing different concentrations of the latter were prepared by ultrasonication route. The X-ray diffraction (XRD) studies and the transmission electron microscopy (TEM) images showed that the synthesized magnetite particles had 80 nm dimensions. The band gap of the composites was evaluated using the UV–visible Spectroscopy. The influence of magnetite content on the magnetic properties of the composite showed a decrease in the saturation magnetization with the decrease in the magnetic content. The effect of magnetite content on the dielectric properties of the polymer film at different frequencies from 0.01 to 105 Hz was studied using an electrochemical impedance spectroscopy. The possible mechanism for the observed electrical properties of the composite films was discussed.

© 2010 Elsevier B.V. All rights reserved.

1. Introduction

Polymer matrix based nanocomposites has become a prominent area of current research and development due to their potential application in biomedicine. Magnetite nanoparticles were incorporated into polymers such as poly(vinyl alcohol) [1], poly(ethylene glycol) [2], poly(acrylic acid) [3], DNA [4], protein [5] and polysaccharide [6] matrix to improve the biocompatibility or bioactivity for biomedical application, such as magnetic cell separation, target drug delivery system and magnetic resonance imaging of clinical diagnosis [7]. Among the various polymers, the biopolymer chitosan has an excellent film forming ability, high mechanical strength, biocompatibility, non-toxicity, high permeability towards water, susceptibility to chemical modifications, cost-effectiveness, etc. Many attempts have been made to improve the biocompatibility and activity of chitosan by structural modification by fabrication of nanocomposites with metal oxide nanoparticles [8,9]. Due to the magnetic nature of these iron oxide-magnetite nanocomposites, they can be used for magnetically targeted cancer therapy [10] or may even improve the delivery and recovery of biomolecules for desired biosensing applications [11,12]. In addition, the nanoparticles have a unique ability to promote fast electron transfer between electrode and the active site of an enzyme, thus further improving the scope as a biosensor [13]. Efforts have recently been made to improve the optical and electrical properties of chitosan for biosensor applications by dispersing superparamagnetic Fe_3O_4 nanoparticles [14].

The objective of the present work was to study the influence of iron oxide nanoparticles on the magnetic and electrical properties of

iron oxide-chitosan composite films. The nanoparticles were primarily prepared by hydrothermal synthesis and then dispersed into the chitosan solution by ultrasonication. The nanoparticles and films are characterized and their magnetic behavior was studied. The dielectric responses of the composites are discussed in relation to material structure and electron transfer between nanoparticles.

2. Experimental studies

All the chemicals such as anhydrous FeCl_3 and $\text{NH}_2 \cdot \text{NH}_2 \cdot \text{HCl}$ used in the preparation of nanomagnetite particles were of analytical grade and used without further purification. Deionized water was used throughout the study.

2.1. Preparation of nano- Fe_3O_4 particles

Hydrothermal synthesis of iron oxide nanoparticles was carried out in a high-temperature, high pressure apparatus called 'autoclaves' or 'bombs' whose internal volume was 20 ml. Hydrazine hydrate (4 mmol) was added to an acidic solution of iron (III) chloride (1 mmol). The solution was stirred for an hour and transferred to the autoclave. The autoclave was then capped and heated in an oven whose temperature was maintained at 473 K for 3 h. The precipitate obtained was centrifuged, washed with absolute alcohol and distilled water and dried at 333 K for 6 h.

2.2. Preparation of chitosan-magnetite films

Medium molecular weight chitosan was dissolved in 2% acetic acid solution (2% m/v). Magnetic particles were dispersed into the

* Corresponding author. Tel.: +91 9481271262.

E-mail address: denthajekb@gmail.com (D. Krishna Bhat).

prepared chitosan-acetic acid solution by ultrasonic irradiation for 60 min. According to the percentage of magnetic particles added, the resulting suspensions were termed as PC, CM1, CM2, CM3 and CM4 for 0%, 10%, 20%, 40% and 50%, respectively. After sonication, the composite blends were poured into a glass plate and dried at 333 K for 6 h. The glass plates were cooled and subsequently immersed in alkali solution to finally get the chitosan-magnetite films. The films were further soaked in distilled water for 24 h to remove the residual solvent.

The X-ray powder diffraction analysis was conducted on a Bruker ASS X-ray diffractometer at a scanning rate of 4° per minute with 2θ ranging from 10° to 90°, using Cu K_{α} radiation ($\lambda=1.5406\text{ \AA}$). The morphological analysis of iron oxide nanoparticles was analyzed using transmission electron microscopy (JEOL 2000 FX). The UV-visible spectroscopy of the composites was performed using a GBC-Cintra 101 spectrophotometer in the

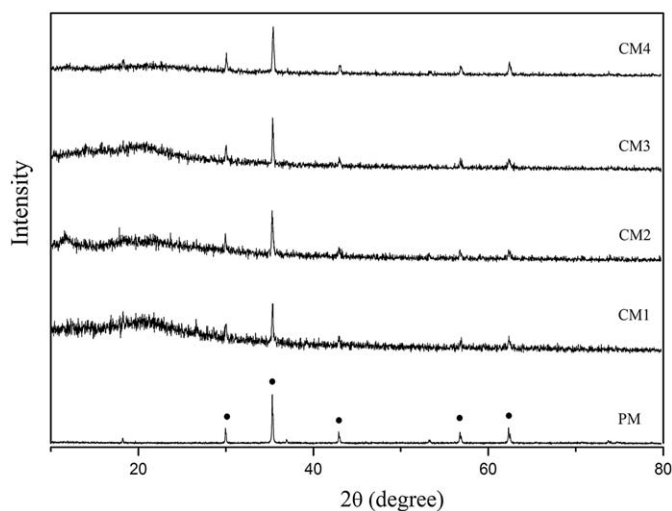
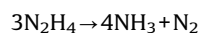


Fig. 1. The XRD pattern of the synthesized magnetite nanoparticles and the composites.

range 200–400 nm. 0.1 M HCl solution was used for the analysis. The magnetic properties were assessed with a vibration sample magnetometer (ADE-DMS EV-7 VSM). From the magnetic saturation and coercivity values, the effect of the nanoparticles was evaluated. Electrochemical measurements were carried out in GAMRY instruments (Series-G750) at room temperature in the presence of phosphate buffer saline (100 mM, pH 7.0, 0.9% NaCl) containing 50 mM $[\text{Fe}(\text{CN})_6]^{3-/4-}$ as the electrolyte. Samples were mounted on the conductivity holder with stainless steel electrodes of diameter 1 cm under spring pressure.

3. Results and discussion

The XRD patterns of magnetite (PM) and chitosan-magnetite films (CM1–CM4) are shown in Fig. 1. PM showed diffraction peaks at $2\theta=30.1^\circ, 35.5^\circ, 43.0^\circ, 57.1^\circ, 62.7^\circ$, which can be indexed to (2 2 0), (3 1 1), (4 0 0), (5 1 1) and (4 0 0) planes of magnetite, respectively. The reflection peaks obtained in this figure are in good agreement with the standard magnetite file (JCPDS no 82-1533), indicating that the sample has a cubic crystalline structure. The average crystallite size obtained from the Scherrer equation was about 80 nm. Also, it was observed that decrease in the amount of hydrazine from 4 to 2 mmol at lower temperatures, resulted in the mixture of $\alpha\text{-Fe}_2\text{O}_3$ and Fe_3O_4 phases. This shows that synthesis temperature as well as the amount of hydrazine hydrate has an influence on the phase of the product. A similar observation was reported by Wang et al. [15]. The formation of single phase Fe_3O_4 particles in presence of higher amount of hydrazine hydrate may be due to the thermal decomposition of the excess hydrazine hydrate at elevated temperature [16].



Nitrogen may protect Fe_3O_4 from further oxidation by air.

Fig. 2 shows the TEM micrograph of iron oxide particles. The TEM analysis of the products provided information on the size and morphology of the nanoparticles. It can be seen from Fig. 2 that the magnetite particles had a hexagonal shape with weak agglomeration.

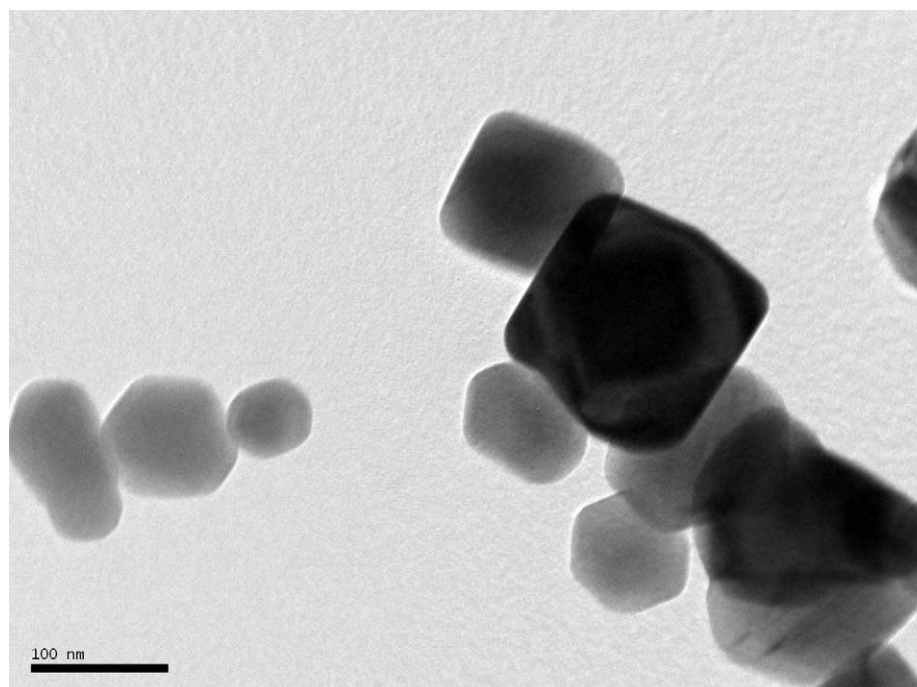


Fig. 2. The TEM image of magnetite nanoparticles.

Fig. 3 shows the absorption spectra of chitosan-magnetite composites. The spectrum of pure chitosan (PC) shows the fundamental absorption edge at 244.48 nm whereas in CM1, CM2, CM3 and CM4 composites the values are found at 276.21, 284.27, 287.97 and 290.46 nm respectively. The band gap values are calculated using the formula $E_a = 1.24/\lambda_{\max}$, where λ_{\max} is the fundamental absorption edge and is presented in Table 1 [17]. The observed red shift may arise from the structural changes and difference in particle sizes [18].

The magnetic properties of the synthesized nanoparticles and films were evaluated using a VSM. The measurements were carried out at room temperature (Fig. 4). The magnetization curve of pure magnetite nanoparticles showed a small hysteresis loop. The saturation magnetization at room temperature was 17.852 emu/g, which is much smaller than that of bulk Fe_3O_4 [19,20]. The magnetic properties of chitosan-magnetite films depend on Fe_3O_4 content as shown in Table 1. Increase in Fe_3O_4 content from 0% to 50% considerably increases the saturation magnetization to 10.31 emu/g. Further, there have been several reports on the decrease in M_s values of composites as iron oxide nanoparticles are embedded into a non-magnetic polymer matrix [21–23]. It is thus obvious that the M_s values of the composites are lower than that of the pure magnetite nanoparticles.

Electrochemical impedance spectroscopy measures impedance of electrode surface as a function of frequency due to variation in interfacial properties of the interface of the electrode electrolyte. The modification of electrode surface results in change in the value of surface electron transfer resistance (R_{CT}). Table 1 lists the R_{CT} values of the samples obtained by fitting the impedance plot with a Randles circuit, wherein the capacitance was treated as a constant phase element (CPE) to average out effects, due to inhomogenities. Fig. 5 shows the Nyquist diagrams of the films in phosphate buffer solution

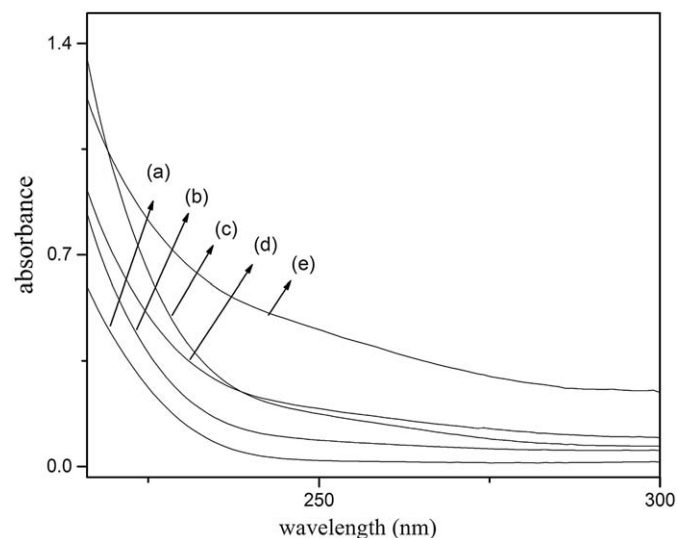


Fig. 3. The UV–visible spectra showing the absorption edge of the samples (a) PC, (b) CM1, (c) CM2, (d) CM3, and (e) CM4.

Table 1
Bandgap, M_s , R_{CT} and σ_{RT} values for pure and composite samples.

Sample	Band gap (eV)	M_s (emu g ⁻¹)	R_{CT} (Kohms)	σ_{RT} (S cm ⁻¹)
PC	5.07	–	234.10×10^4	3.40×10^{-13}
CM1	4.49	6.00	299.80	2.97×10^{-9}
CM2	4.36	7.59	176.30	5.78×10^{-9}
CM3	4.31	8.63	83.46	1.14×10^{-8}
CM4	4.27	10.31	8.23	1.24×10^{-7}
PM	–	17.85	–	–

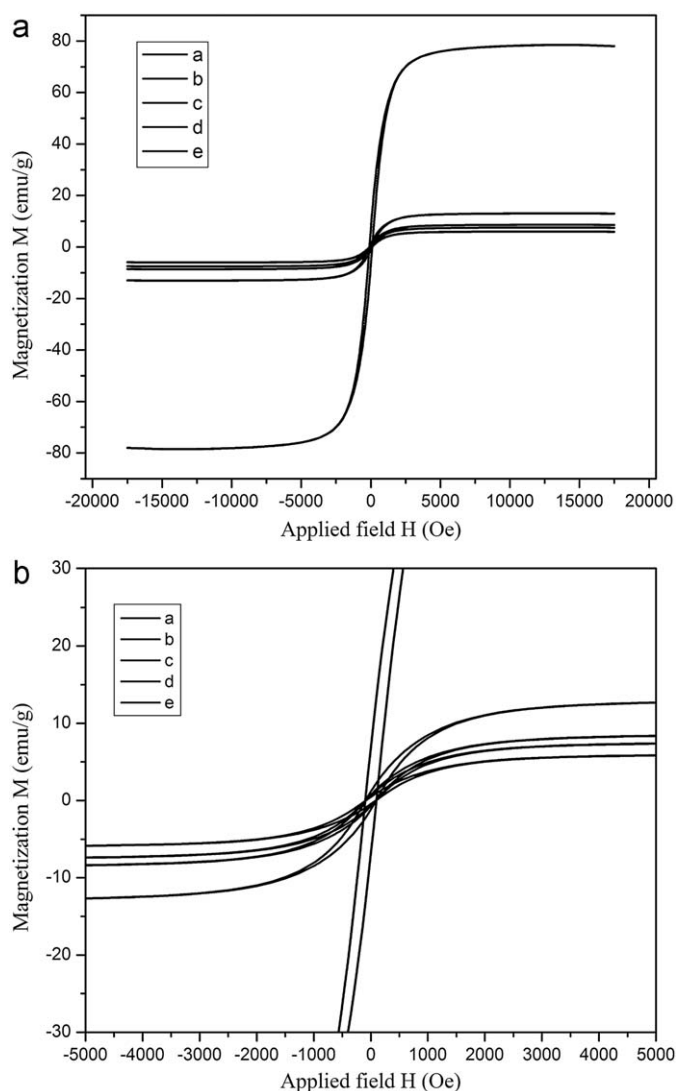


Fig. 4. (a) Room temperature magnetization curves for (a) CM1, (b) CM2, (c) CM3, (d) CM4, and (e) PM and (b) enlarged view.

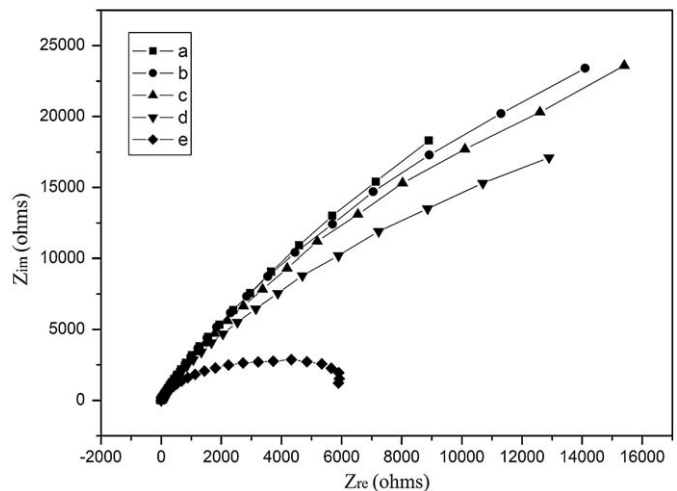


Fig. 5. Nyquist plot for the samples (a) PC, (b) CM1, (c) CM2, (d) CM3, and (e) CM4.

in the frequency range from 0.01 to 10^5 Hz at room temperature. It is observed that R_{CT} obtained for chitosan decreases as the magnetite content increases. This suggests that for chitosan films embedded

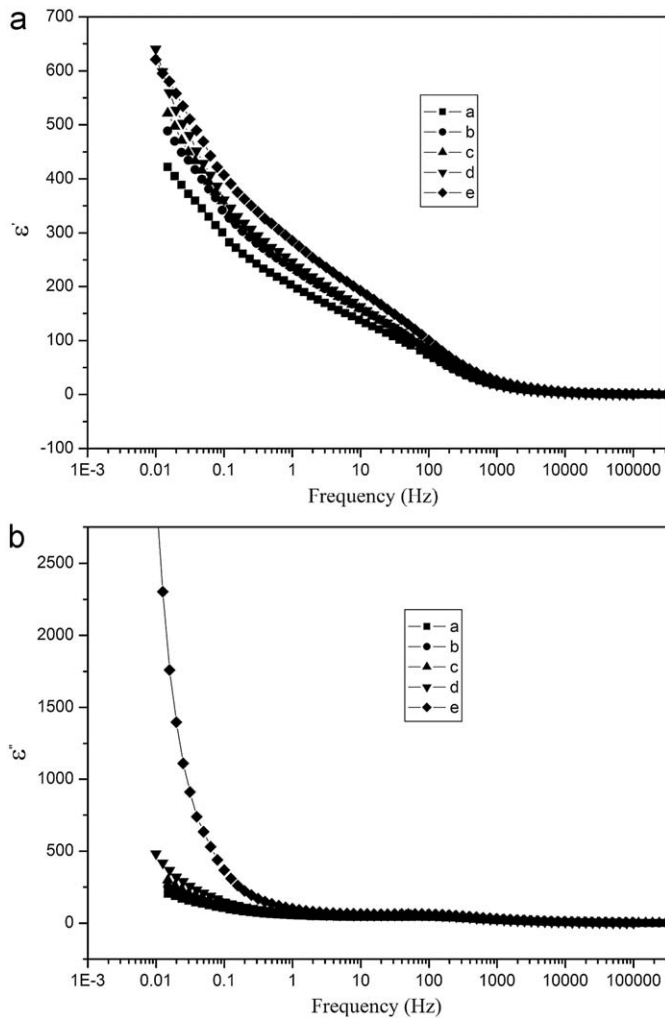


Fig. 6. a. Dielectric constant as function of frequency for the samples (a) PC, (b) CM1, (c) CM2, (d) CM3, and (e) CM4. and (b) dielectric loss as a function of frequency for the samples (a) PC, (b) CM1, (c) CM2, (d) CM3, and (e) CM4.

with magnetite, electron transfer is easier between solution and the electrode due to the permeable structure of the chitosan polymer [13]. As expected, the conductivity of the samples increased with increase in the magnetite content in the polymer film (Table 1). The bulk ionic conductivities (σ) were determined from the complex impedance spectra using the equation, $\sigma = L/RA$ where L , A and R are respectively, the thickness, area and bulk resistance of the samples. The bulk resistance was calculated from the high frequency intercept on the real impedance axis of the Nyquist plot [24].

Complex impedance data, Z^* , can be represented by its real, Z_R and imaginary, Z_I parts by the relation

$$Z^* = Z_R + jZ_I \quad (1)$$

The equations for the dielectric constant, ϵ_R and the dielectric loss, ϵ_I can be shown as

$$\epsilon_R = \frac{Z_I}{\omega C_0 (Z_R^2 + Z_I^2)} \quad (2)$$

$$\epsilon_I = \frac{Z_R}{\omega C_0 (Z_R^2 + Z_I^2)} \quad (3)$$

Here $C_0 = \epsilon_0 A/t$ and ϵ_0 is the permittivity of free space, A is the electrolyte–electrode contact area and t is the thickness of the sample and $\omega = 2\pi f$, f being the frequency in Hz.

Figs. 6(a) and (b) shows respectively the dielectric constant (ϵ') and the dielectric loss (ϵ'') of the films with varying frequencies. Dielectric constant describes the stored energy while the dielectric loss describes the dissipated energy. It is clear from the figure that both ϵ' and ϵ'' decreased with increase in frequency for all the samples. However, the decrease in ϵ' is more rapid than in ϵ'' . In the high frequency range (above 10^3 Hz) the values of ϵ' become closer to the values of ϵ'' . Also, no appreciable relaxation peaks are observed in the frequency range employed in the study.

The decrease in dielectric constant with increase in frequency is due to the fact that the polarization decreases and then reaches a constant value beyond a certain frequency limit (higher frequencies). The variation in dielectric constant with frequency clearly reveals that the dispersion exhibited by the samples is due to the Maxwell–Wagner type of interfacial polarization and in agreement with Koop's phenomenological theory [25–27]. This behavior can be explained by assuming the mechanism of dielectric polarization, which is similar to that of conduction mechanism [28].

The $\text{Fe}^{2+} \leftrightarrow \text{Fe}^{3+}$ electron exchange results in the local displacement of charges in the direction of an applied electric field, which is responsible for polarization in ferrites [26]. The polarization decreases with increase in frequency of the externally applied electric field and the electronic exchange between Fe^{2+} and Fe^{3+} is independent of variations in applied field, thereby resulting in decrease in dielectric constant. The magnitude of exchange depends on the concentration of $\text{Fe}^{3+}/\text{Fe}^{2+}$ ion pairs present at the B-site.

4. Conclusions

In summary, crystalline magnetite nanoparticles were prepared and embedded in the chitosan polymer. The optical band gap values of the composites showed a red shift, which confirmed the dispersion of the magnetic filler in the polymer matrix. The saturated magnetization of the composite films could reach a value of 10.31 emu/g with 50% doping of magnetite. The impedance spectroscopy results show that the presence of nanoparticles eases the electron transfer between the solution and the electrode and the R_{CT} value goes as low as 8.23 ohms. The nanocomposites may apply to the magnetic field assisted drug delivery systems, cell/enzyme immobilization, biosensors and many other industrial processes.

Acknowledgement

We gratefully acknowledge DST, India for their financial support in the form of an R&D project grant. We also like to thank Mr. Sivakumar, Indian Institute of Technology, Kanpur for helping us with magnetic measurements. ASB is grateful to NITK Surathkal for the award of a research fellowship.

References

- [1] A. Sinha, J. Chakraborty, S.K. Das, S. Das, V. Rao, P. Ramachandrarao, Mater. Trans. 42 (2001) 1672.
- [2] Y. Zhang, N. Kohler, M. Zhang, Biomaterials 23 (2002) 1553.
- [3] S. Si, A. Kotal, T.K. Mandal, S. Giri, H. Nakamura, T. Kohara, Chem. Mater. 16 (2004) 3489.
- [4] S. Mornet, A. Vekris, J. Bonnet, E. Duguet, F. Grasset, J.H. Choy, J. Portier, Mater. Lett. 42 (2000) 183.
- [5] M. Allen, D. Willits, J. Mosolf, M. Young, T. Douglas, Adv. Mater. 14 (2002) 1562.
- [6] P. Sipos, O. Berkseri, E. Tombacz, T.G.S. Pierre, J. Webb, J. Inorg. Biochem. 95 (2003) 55.
- [7] D. Bahadur, J. Giri, Sadhana 28 (2003) 639.
- [8] Y. Miao, S.N. Tan, Analyst 125 (2000) 1591.
- [9] C. Xu, H. Cai, P. He, Y. Fang, Analyst 126 (2001) 62.

- [10] T. Neuberger, B. Schopf, H. Hofmann, M. Hofmann, B. van Rechenberg, *J. Magn. Magn. Mater.* 293 (2005) 483.
- [11] A. Kaushik, R. Khan, P.R. Solanki, P. Pandey, J. Alam, S. Ahmad, B.D. Malhotra, *Biosens. Bioelectron.* 24 (2008) 676.
- [12] G.K. Kouassi, J. Irudayaraj, G. McCarty, *J. Nanobiotechnol.* 3 (2005) 1.
- [13] A. Kaushik, P.R. Solanki, A.A. Ansari, G. Sumana, S. Ahmad, B.D. Malhotra, *Sensor. Actuat. B—Chem.* 138 (2009) 572.
- [14] A. Kaushik, P.R. Solanki, A.A. Ansari, S. Ahmad, B.D. Malhotra, *Electrochem. Commun.* 10 (2008) 1364.
- [15] W.W. Wang, Y.J. Zhu, M.L. Ruan, *J. Nanopart. Res.* 9 (2007) 419.
- [16] P. Patnaik, *Handbook of Inorganic Chemistry*, The McGraw Hill Companies, 2002, p. 344.
- [17] S.E. Dali, M.J. Chockalingam, *Mater. Chem. Phys.* 70 (2001) 73.
- [18] S. Balaji, R.K. Selvan, L.J. Berchmans, S. Angappan, K. Subramanian, C.O. Augustin, *Mater. Sci. Eng. B* 119 (2005) 119.
- [19] K.V.P. Shafi, A. Ulman, A. Dyal, X.Z. Yan, N.L. Yang, C. Estournes, L. Fournes, A. Wattiaux, H. White, M. Rafailovich, *Chem. Mater.* 14 (2002) 1778.
- [20] M. Mikhaylova, D.K. Kim, N. Bobrysheva, M. Osmolowsky, V. Semenov, T. Tsakalacos, M. Muhammed, *Langmuir* 240 (2004) 2472.
- [21] J. Yang, S.B. Park, H.G. Yoon, Y.M. Huh, S. Haam, *Int. J. Pharm.* 324 (2006) 185.
- [22] L. Cui, H. Gu, H. Xu, D. Shi, *Mater. Lett.* 60 (2006) 2929.
- [23] S.E. Jacobo, J.C. Apesteguy, R.L. Anton, N.N. Schegoleva, G.V. Kurlyandskaya, *Eur. Polym. J.* 43 (2007) 1333.
- [24] N.A. Choudhury, A.K. Shukla, S. Sampath, S. Pitchumani, *J. Electrochem. Soc.* 103 (2006) A614.
- [25] C.G. Koops, *Phys. Rev.* 83 (1951) 121.
- [26] J.C. Maxwell, *A Treatise on Electricity and Magnetism*, vol. 1, Oxford Press, London, 1973, p. 828.
- [27] K. Iwachi, *Jpn. J. Appl. Phys.* 10 (1971) 1520.
- [28] R.R. Heikes, W.D. Johnson, *J. Chem. Phys.* 26 (1957) 582.